

# TMT-AGE: wide field of regard multi-object adaptive optics for TMT

Masayuki Akiyama<sup>a</sup>, Shin Oya<sup>b</sup>, Yoshito H. Ono<sup>a,b</sup>, Hideki Takami<sup>c</sup>, Shinobu Ozaki<sup>c</sup>, Yutaka Hayano<sup>b</sup>, Ikuru Iwata<sup>b</sup>, Kazuhiro Hane<sup>d</sup>, Tong Wu<sup>d</sup>, Tomoyasu Yamamuro<sup>e</sup> and Yuji Ikeda<sup>f</sup>

<sup>a</sup>Astronomical Institute, Tohoku University, 6-3 Aramaki, Aoba-ku, Sendai, Japan;

<sup>b</sup>Subaru Telescope, National Astronomical Observatory of Japan, 650 North A'ohoku Place, Hilo, HI, USA;

<sup>c</sup>National Astronomical Observatory of Japan, 2-21-1 Osawa, Mitaka, Tokyo, Japan;

<sup>d</sup>Department of Nanomechanics, Tohoku University, 6-6 Aramaki, Aoba-ku, Sendai, Japan;

<sup>e</sup>OptCraft, 3-16-8-101 Higashi-Hashimoto, Midori-ku, Sagami-hara, Japan;

<sup>f</sup>Photocoding Inc., 460-102 Iwakura-Nakamachi, Sakyo-ku, Kyoto, Japan;

## ABSTRACT

We introduce current status of the feasibility study on a wide field of regard (FoR) Multi-Object Adaptive Optics (MOAO) system for TMT (TMT-AGE: TMT-Analyzer for Galaxies in the Early universe). MOAO is a system which realize high spatial-resolution observations of multiple objects scattered in a wide FoR. In this study, we put emphasise on the FoR as wide as 10' diameter. The wide FoR is crucial to effectively observe very high-redshift galaxies, which have low surface number density. Simulations of an MOAO system with 8 LGSs show close-to-diffraction-limited correction can be achieved within 5' diameter FoR and moderate AO correction can be achieved within 10' diameter FoR. We discuss overall system design of the wide FoR MOAO system considering the constraint from the stroke of small-size deformable mirror (DM). We also introduce current status of developments of key components of an MOAO system; high-dynamic range wavefront sensor (WFS) and large-stroke small-size DM, and real time computer (RTC) with fast tomographic reconstruction.

**Keywords:** Adaptive Optics, TMT, Multi-Object Adaptive Optics, simulation

## 1. INTRODUCTION

Multi-Object Adaptive Optics (MOAO) is an AO system that delivers close-to diffraction-limited images of multiple objects scattered in a wide Field of Regard (FoR) simultaneously.<sup>1</sup> The 3D volume structure of the atmospheric turbulence is estimated by tomographic reconstruction with wavefront measurements of multiple laser guide stars (LGSs). The estimated 3D structure of the atmospheric turbulence is integrated along the line-of-sight of each target and the optimised correction for each target is determined. Multiple targets are picked up by multiple science paths. The optimised correction for each science path is applied to a deformable mirror (DM) in the science path. The control of the DM is made in open-loop manner. Because Tip-Tilt (TT) and focus components cannot be sensed with the LGSs, natural guide stars (NGSs) are necessary to measure the components. Because TT component also has anisoplanatism, we need multiple NGSs within the wide FoR to estimate TT component of each science path. Bright NGSs within the wide FoR can also be used for high-order wavefront measurements.<sup>2</sup>

Multiple deployable integral field units (IFUs) assisted with the MOAO system is a powerful instrument to obtain high-resolution 3D (two spatial and one wavelength dimension) information of statistical number of galaxies. For Thirty Meter Telescope (TMT), two feasibility studies have been done for MOAO-assisted multiple-IFUs NIR spectrograph under the name of Infrared Multi-Object Spectrograph (IRMOS).<sup>3</sup> One is done by members of University of Florida (UF) and Herzberg Institute of Astrophysics (HIA), IRMOS-UF/HIA concept<sup>4-6</sup> and the other one done by members of Caltech and Laboratoire d'Astrophysique de Marseille (LAM),

---

Further author information: (Send correspondence to M.A.)

M.A.: E-mail: akiyama@astr.tohoku.ac.jp, Telephone: +81 (0)22 795 6511

Adaptive Optics Systems IV, edited by Enrico Marchetti, Laird M. Close,  
Jean-Pierre Véran, Proc. of SPIE Vol. 9148, 914814 · © 2014 SPIE  
CCC code: 0277-786X/14/\$18 · doi: 10.1117/12.2056320

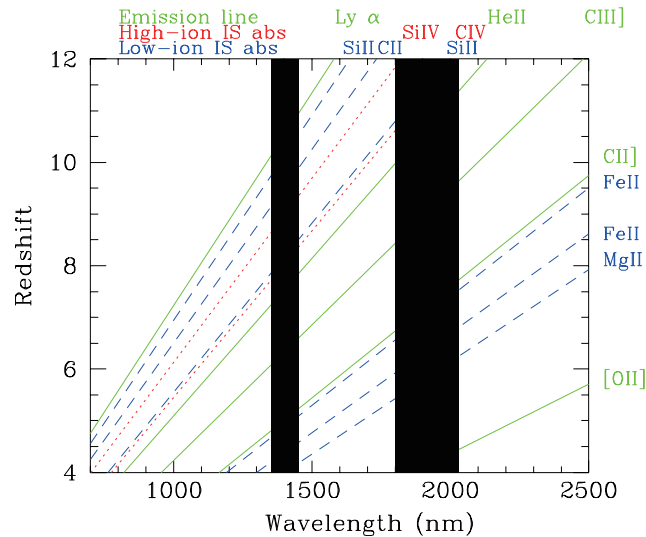


Figure 1. Observed wavelength of strong rest-frame UV lines for galaxies at  $z = 5-12$ . Green solid lines, blue dashed lines, and red dotted lines represents strong emission, low-ionization inter-stellar absorption, and high-ionization inter-stellar absorption lines observed in Lyman Break Galaxies at  $z \sim 3$ <sup>8</sup> and galaxies at  $z \sim 2$ .<sup>9</sup>

IRMOS-Tipi concept.<sup>7</sup> Both of these feasibility studies conducted following the IRMOS specification with near diffraction-limited PSF within  $5'$  diameter FoR.

Following the feasibility studies on IRMOS, we started a feasibility study of an MOAO system covering even wider FoR up to  $10'$  diameter under the name of TMT-AGE (TMT-Analyzer for Galaxies in the Early universe). The wide FoR is crucial to effectively observe very high-redshift galaxies at  $z > 5$ , whose surface number density is rather low. In this paper, we describe the science drivers for a wide FoR MOAO system and MOAO performance simulations in the wide FoR. Then, we describe overall system considerations emphasising requirements for DMs. Finally we mention on-going developments related to components of the MOAO system; high dynamic range wavefront sensors (WFS), large stroke DMs, and fast tomography real time controller.

## 2. SCIENCE DRIVERS AND AO PERFORMANCE FEASIBILITY

### 2.1 Exploring the galaxies in the high-redshift universe with an ELT MOAO system

In this study, we put emphasis on the three science cases that can be tackled with an ELT MOAO system; 1) revealing the history of establishment of the internal structure of galaxies, 2) revealing the physical process associated with the violent star-formation during the formation phase of galaxies, and 3) identifying the galaxies in the early universe.

For the first science case, the history of the establishment of the internal structure of galaxies seen in the current universe, i.e. Hubble sequence, will be revealed by spatially resolved spectroscopy of galaxies at up to redshift 5. Recent studies on morphology of galaxies in the high-redshift universe<sup>10</sup> suggest that morphological mixture of galaxies at  $z > 1$  is different from that seen in the local universe. Dynamical structure of the galaxies at  $z \sim 1-2$  is also different, they show systematic rotation, like disk galaxies in the local universe, but they have large velocity dispersion component as well.<sup>11</sup> High-spatial and high-sensitivity observations supported by AO system on ELT is crucial to reveal gas dynamics, gas metallicity, and stellar populations in each region of the high-redshift galaxies. The average half-light radius of galaxies at redshifts  $z = 2$  and  $4$  are  $2.5$  and  $1.5$  kpc,<sup>12</sup> which are  $0.3''$  and  $0.2''$  for each redshift. In reality, the dynamical structure of a galaxy at  $z \sim 3$  revealed thanks to Gravitational lensing effect shows steep velocity gradient within  $1$  kpc scale.<sup>13</sup> In order to resolve such structure of galaxies at  $z = 2-4$  with at least 3 spatial elements, spatial resolution as small as  $0.05'' \times 0.05''$  is necessary.<sup>5</sup> Moreover, considering the diversity of the physical properties of galaxies, observations of statistical number of high-redshift galaxies are important.

For the second science case, the physical process of violent star-formation in the very high-redshift galaxies at  $z > 5$  will be addressed by observing their integrated rest-frame UV spectra. Rest-frame UV emission and absorption lines of star-forming galaxies provide us important information on the properties of high-mass star-formation and inflowing and outflowing gas associated with the galaxies.<sup>8</sup> Strength of the HeII emission line can be used to constrain the slope of initial mass function in the high-mass end. The strength and velocity of low-ionization and high-ionization inter-stellar absorption lines can be used to constrain the distribution and kinematics of neutral and ionized gas around the galaxies. The observed wavelength of the redshifted UV lines are summarised in Figure 1. Most of the strong UV lines of very high-redshift galaxies can be observed in the  $J$ - and  $H$ -bands up to redshift 10, and high-sensitivity spectroscopy of faint galaxies is crucial for this science case. The observed circularized half-light radius of the UV-luminous ( $M_{UV} < -20\text{mag}$ ) galaxies at  $z \sim 7 - 8$  is 0.6 kpc in the rest-frame UV wavelength,<sup>14</sup> which corresponds to  $0.11''$ . For UV-luminous galaxies at  $z \sim 10$ , the half-light radius can be as small as 0.3 kpc,<sup>14</sup> which is  $0.07''$ . They are much smaller than typical seeing size at Mauna Kea, and moderate AO correction can help significantly improve the sensitivity for integrated spectroscopy under the sky-background limited condition. The equivalent width of these rest-frame UV absorption lines are  $1 \sim 2 \text{ \AA}$  in the rest-frame, therefore spectroscopy with moderate resolution with  $R \sim 1,000$  is important.

The targets for the third science case are candidates of galaxies in the early universe found by ALMA and future wide-field NIR survey satellite missions, like Euclid, WFIRST, and WISH. For example, Ultra Deep Survey of WISH will cover  $100 \text{ deg}^2$  down to 28 AB magnitude in  $1\text{-}5\mu\text{m}$  (wishmission.org) with  $3\sigma$  and provide candidates of galaxies at  $z \geq 8$ . These candidates can be identified with  $\text{Ly}\alpha$  emission line in NIR (Figure 1). Considering the strong redshift evolution of  $\text{Ly}\alpha$  emission line luminosity function of galaxies possibly due to high neutral fraction in the early universe,<sup>15</sup> we may need to identify the candidates with absorption lines and continuum break.

In Figure 2, detection limits of  $J$ -,  $H$ -,  $K$ -band spectroscopic observations with TMT are summarised. We compare the detection limit of  $R = 500$  spectroscopy with MOAO PSF, moderately-corrected PSF by Ground-layer Adaptive Optics (GLAO) system, and seeing-limited PSF. The PSFs are evaluated with average of PSFs within  $5'$  diameter field corrected by each AO mode. We assume fixed square aperture observation, and the horizontal axis represent the area of the fixed aperture. Ensquared Energy (EE) is calculated for each PSF. For the point source observation (left panel) MOAO PSF with small aperture can achieve highly sensitive observations thanks to the reduced background emission. On the other hand, for the extended galaxies (right panel), because their sizes are larger than the diffraction-limit PSF, reducing the size of the aperture do not help to increase sensitivity. GLAO-like moderately corrected observations with  $0.1''\text{-}0.2''$  aperture can be only  $\sim 0.2\text{mag}$  shallower than observations with MOAO PSF. As can be seen in Figure 1,  $J$ -band observations are important for the second and third science cases.  $R = 500$  fixed aperture spectroscopy with MOAO and GLAO modes can reach 25.7 and 25.6 mag with  $\text{SN}=10$  with 10h integration in the  $J$ -band. The expected sensitivities can be fainter than those of NIRSpec on James Webb Space Telescope (JWST):  $J_{AB} = 25.2\text{mag}$  with  $R = 1,000$  and  $\text{SN}=10$  in 27.7h integration within  $3' \times 3'$  FoV (NIRSpec pocket guide), therefore moderate resolution spectroscopy of faint galaxies supported by wide-field AO correction can be one of the unique capability of ground-based TMT.

The sensitivity for spatially-resolved emission-line spectroscopy is also estimated with the same assumption used in Figure 2. The limits for flux density and line flux are summarized in Table 1. The detection limits for line flux are derived assuming the lines are not resolved with the resolution. The  $J$ -,  $H$ - and  $K$ -band detection limits for line flux with  $R = 3,000$  are  $2.5 \times 10^{-20}$ ,  $1.7 \times 10^{-20}$ ,  $3.6 \times 10^{-20} \text{ erg s}^{-1} \text{ cm}^{-2}$  per  $0.05'' \times 0.05''$  spatial pixel with  $\text{SN}=10$  by 10h integration. The detection limit corresponds to  $\text{H}\alpha$  emission line of  $0.002 M_{\odot} \text{ yr}^{-1}$  and  $0.01 M_{\odot} \text{ yr}^{-1}$  per spatial pixel for galaxies at  $z = 1.5$  and  $z = 2.5$ , respectively.

The number densities of the targets for the second and third science cases are not very high. For example the number densities of the UV-bright  $z \geq 5$  galaxies that are brighter than the detection limits are 0.41 per  $\text{arcmin}^2$  for  $z \sim 5$  galaxies with  $Y < 25.5\text{mag}$  picked up by  $V$ -dropout method, 0.17 per  $\text{arcmin}^2$  for  $z \sim 6$  galaxies with  $Y < 25.9\text{mag}$  picked up by  $i$ -dropout method, and 0.10 per  $\text{arcmin}^2$  for  $z \sim 7$  galaxies with  $J < 26.0\text{mag}$  picked up by  $z$ -dropout method.<sup>16</sup> The expected number density of the candidates of very high-redshift galaxies at  $z \geq 8$  is 0.5 per  $\text{arcmin}^2$ . Considering the low surface number density, wide FoR as wide as  $10'$  diameter is crucial to achieve efficient observations of statistical number of very high-redshift galaxies utilising high multiplicity of an MOAO system: 0.25 targets per  $\text{arcmin}^2$  is required to effectively feed 20 science paths per  $10'$  diameter FoR.

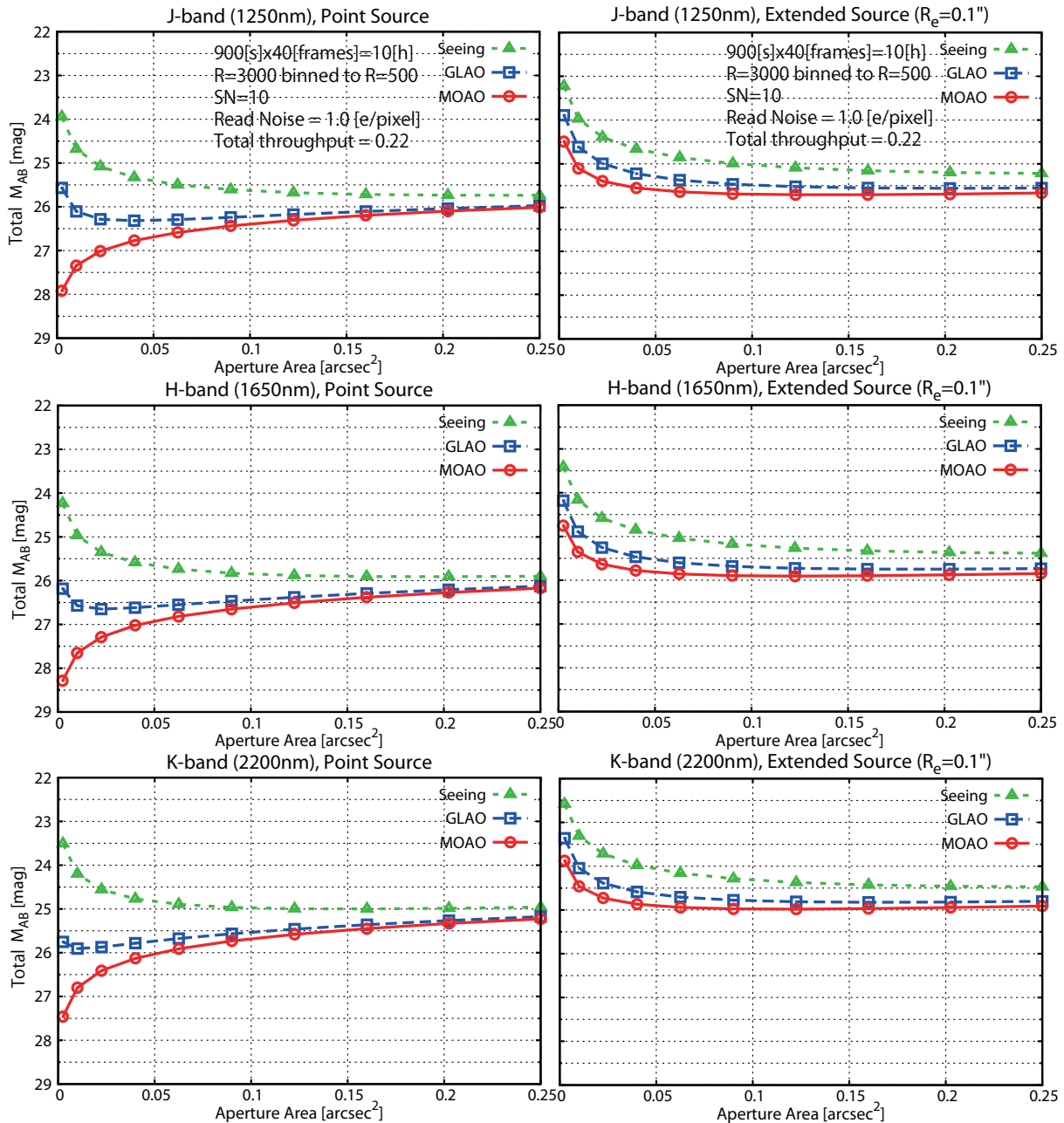


Figure 2. *J*-, *H*-, *K*-bands magnitude limits of spectroscopic observations with TMT MOAO, GLAO, and seeing-limited observations. The horizontal axis represents area of square aperture on the sky, i.e.  $0.04 \text{ arcsec}^2$  corresponds to  $0.2'' \times 0.2''$  aperture. We assume fixed aperture spectroscopy to obtain an integrated spectrum. Spatial sampling on the detector is fixed with  $0.025''$  per pixel. EE in the aperture for each AO mode is calculated with average PSF shape within  $5'$  diameter field. In the calculation, the continuum sky-background emission is considered, we assume observation between strong OH-airglow lines with moderate spectroscopic resolution with  $R \sim 3,000$ , and binnig down to  $R \sim 500$  after the removal of the effect of the OH-airglow. Total throughput, including telescope, AO-system, IFU, spectrograph and detector quantum efficiency, of 0.22 is assumed. Left) For point sources, Right) extended galaxy with effective radius of  $0.1''$  exponential-law, i.e. disk-like, galaxies.

Table 1. Detection limits for spatially-resolved spectroscopy with  $0.05'' \times 0.05''$  aperture. We assume extended source that have constant surface brightness and limits are for flux density and line flux within the aperture with SN=10 and 10h integration. Other assumptions are same as in Figure 2

	$J(1250\text{nm})$	$H(1650\text{nm})$	$K(2200\text{nm})$
$R = 3,000$ flux density ( $\text{erg s}^{-1} \text{cm}^{-2} \text{Hz}^{-1}$ )	$3.2 \times 10^{-31}$	$2.9 \times 10^{-31}$	$7.7 \times 10^{-31}$
$R = 3,000$ line flux ( $\text{erg s}^{-1} \text{cm}^{-2}$ )	$2.5 \times 10^{-20}$	$1.7 \times 10^{-20}$	$3.6 \times 10^{-20}$
$R = 500$ flux density ( $\text{erg s}^{-1} \text{cm}^{-2} \text{Hz}^{-1}$ )	$1.2 \times 10^{-31}$	$1.1 \times 10^{-31}$	$2.7 \times 10^{-31}$
$R = 500$ line flux ( $\text{erg s}^{-1} \text{cm}^{-2}$ )	$5.8 \times 10^{-20}$	$4.0 \times 10^{-20}$	$7.0 \times 10^{-20}$

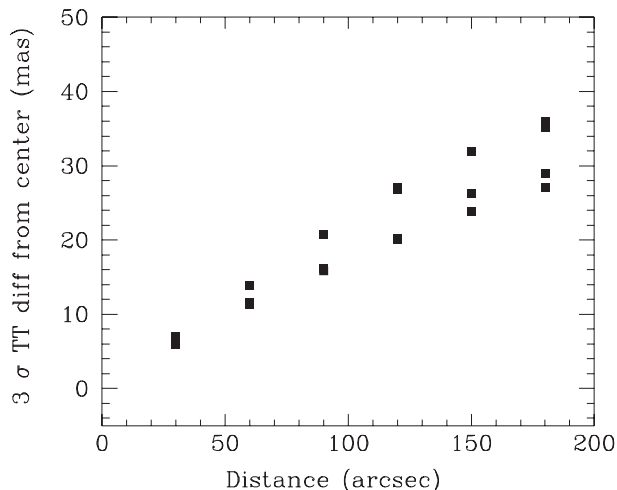


Figure 3. Tip-Tilt anisoplanatism as a function of distance from a guide star. The vertical axis is the  $3 \sigma$  scatter of differences of TT component from the center in each simulation run. Different points at the same distance represent results from different simulation runs.

## 2.2 AO performance simulation within a wide FoR

The performance of an MOAO system in wide FoR is evaluated through AO simulation. The critical parameter of an MOAO system is the configuration of LGSs and NGSs. Laser Guide Star Facility (LGSF) for TMT is designed to support the early-light AO system, NFIRAOS (Narrow Field InfraRed Adaptive Optics System<sup>17</sup>), with 6 LGSs with 1 at the center and 5 equally spaced on a circle with radius of  $35''$ . The LGSF is designed to accept future upgrades with 9 LGSs radii up to  $510''$ .<sup>18</sup> Nominal asterism considered for the TMT-IRMOS system is 3 equally spaced on a circle with radius of  $70''$  and 5 equally spaced on a circle with radius of  $150''$  (Subsystem Requirements Document for the Laser Guide Star Facility as of 2010 Apr.). In the current study, we simulate two patterns, 1) 5 LGSs on a circle and one LGS at its center, and 3 NGSs on a triangle, and 2) 3 LGSs on a inner circle and 5 LGSs on a outer circle, and 3 NGSs on a triangle, as shown in Figure 4. We change the radius of the LGS asterisms from  $140''$  to  $280''$ . The smallest asterism with 8 LGSs corresponds to that of the nominal TMT-IRMOS case.

In both patterns, we use NGSs for measuring TT and focus components only. We locate three NGSs in a triangle with  $r = 120''$  in the simulations. Figure 3 shows amount of TT anisoplanatism as a function of distance determined with the simulations described below. In order to keep the TT error as small as  $0.025''$ , we need a TT guide star within  $120''$ . The number density of 3 NGSs within the  $d = 5'$  FoR corresponds to 550 per  $\text{deg}^2$ . We estimate number density of stars based on the Galaxy star count model TRILEGAL.<sup>19</sup> In the high-galactic latitude regions, stars as faint as  $R_{AB} = 17.5\text{mag}$ ,  $J_{AB} = 15.5\text{mag}$ , and  $K_{AB} = 15.0\text{mag}$  have the required surface number density.

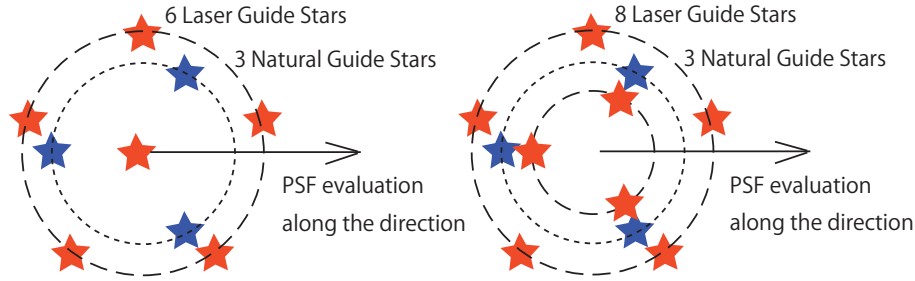


Figure 4. The configuration of the LGSs and NGSs in the performance simulations. We assume 6 LGSs at the center and pentagon, and 3 NGSs at the triangle, the radius of the configuration is changed. The PSFs are evaluated along the evaluation direction.

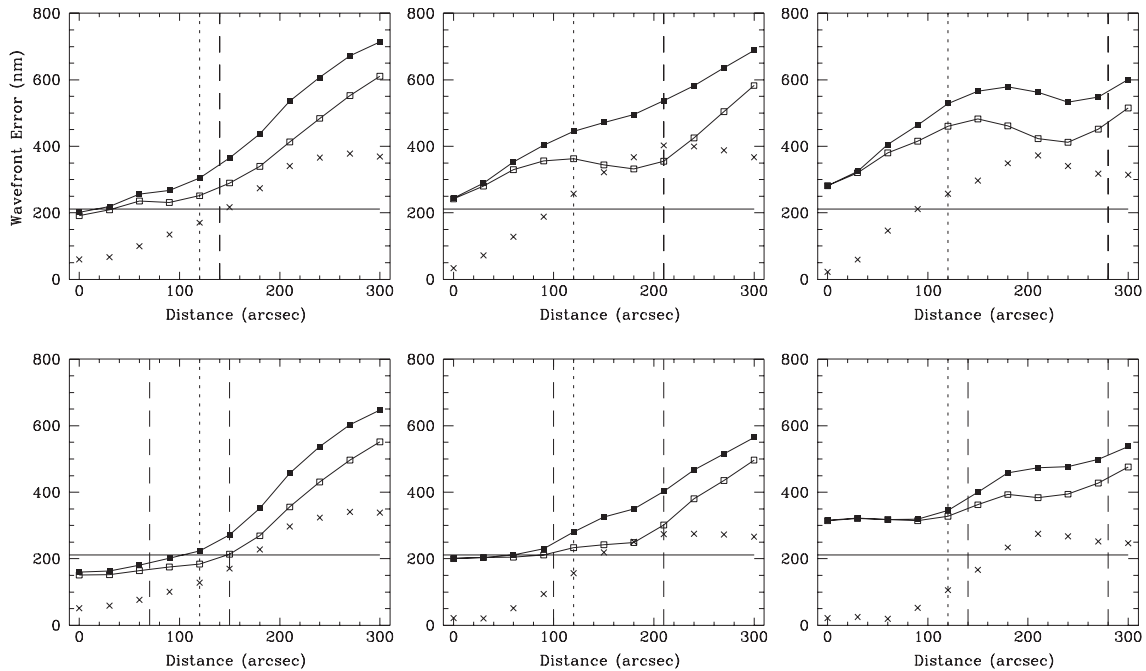


Figure 5. RMS wavefront error (WFE) as a function of distance from the FoR center. Filled squares, crosses, and open squares represent total WFE, TT WFE, and WFE without TT component, respectively. The horizontal solid line indicate WFE of which corresponds to Strehl ratio of 0.5 in the  $H$ -band. The vertical dashed and dotted lines represent radius of LGSs and NGSs asterism. For the top row, one LGS at the center and 5 LGSs on a circle with radius of 140", 175", and 280" from left to right. For the bottom row, 3 LGSs and 5 LGSs on circles with radii of (70" and 150"), (100" and 210"), and (140" and 280"). In all cases, 3 NGSs are located at 120" from the center. The lower left panel corresponds to the nominal TMT-IRMOS LGS configuration.

The simulations are conducted with Multi-threaded Adaptive Optics Simulator (MAOS) AO simulation code.<sup>20</sup> We assume moderate seeing condition with  $r_0 = 0.186\text{m}$  at 500nm and 7 layer turbulence for 13N TMT site on Mauna Kea. Turbulence outer scale  $L_0$  of 30m is assumed in all of the simulations. The 7 layer model has layers at 0m and 500m to represent ground layer turbulence component. Further consideration of the effect of the detailed modelling of the ground layer profile<sup>21</sup> to the wide FoR performance will be made in future. The performance evaluation is done along the direction shown with an arrow in the figure.

The wavefront error (WFE) as a function of distance from the FoR center is shown in Figure 5. We show the total WFE (filled squares) as well as TT WFE (crosses) and WFE after removal of TT WFE (open square). In the TMT-IRMOS study,  $0.05'' \times 0.05''$  EE larger than 50% in the  $H$ -band is considered as scientific requirement.<sup>5</sup>

50% EE within  $0.05'' \times 0.05''$  aperture typically corresponds to Strehl Ratio (SR) of 0.5.<sup>22</sup> SR of 0.5 in the *J*-, *H*-, and *K*-bands corresponds to rms WFE of 159nm, 211nm, and 291nm, respectively. The criteria in the *H*-band is shown with horizontal solid lines in the panels. The criteria can be met with the TMT-IRMOS LGS asterism within  $120''$  from the center. If a wider configuration of LGSs is assumed, the TT-removed WFE in the outer region become smaller, but TT-removed WFE in the central region become larger.

EE within  $0.05'' \times 0.05''$  aperture is shown in Figure 6 as a function of distance from the center.  $0.9\mu\text{m}$ , *J*-, *H*-, and *K*-band EE are shown with crosses, open squares, filled squares, and open circles, respectively. Diffraction-limited PSF have 0.92, 0.90, 0.89, 0.85 EE in  $0.9\mu\text{m}$ , *J*-, *H*-, and *K*-bands, respectively. More than 50% EE in the aperture in the *H*-band within  $5'$  diameter FoR can be achieved only with the nominal TMT-IRMOS configuration as expected from the WFE plot. This is consistent with previous studies.<sup>6</sup> In the *K*-band, more than 50% EE within  $0.05'' \times 0.05''$  EE can be achieved within  $6.5'$  diameter FoR if we use wider asterism with 8 LGSs.

EE in wider aperture with  $0.2'' \times 0.2''$  is shown in Figure 7. More than 50% EE can be achieved almost all regions within  $10'$  diameter FoR in the wavelength range longer than *J*-band with 8 LGSs. The nominal TMT-IRMOS configuration on the lower left panel shows the best results in the almost entire FoR. The EE is 2.5 times larger than the seeing-limited case (0.14, 0.21, 0.21, 0.27 for  $0.9\mu\text{m}$ , *J*, *H*, *K*-bands) even at the edge of the FoR.

These AO simulation results show, we can achieve good AO correction within  $5'$  diameter FoV and moderate AO correction within  $10'$  diameter FoV with standard tomographic reconstruction method with 8 LGSs configured within  $150''$  radius.

We are also considering the atmospheric tomography algorithm that utilise WFS measurement at previous time steps with the wind profile as a function of altitude.<sup>23</sup> The current simulation results of the algorithm are promising: better AO correction than standard tomography can be achieved within  $8'$  diameter FoR with equally spacing 5 LGSs on the  $270''$  circle and 3 LGSs on the  $120''$  circle. The assumed condition is rather ideal in the current simulations; turbulence layer heights are known and perfectly frozen flow holds within 0.1s. Although further realistic simulations with information on the accuracy of estimation of the heights of the turbulence layers and the frozen flow time-scale, the results show there is a possibility that better AO correction can be made in the wide  $10'$  diameter FoR. Details of the algorithm and the simulation results, see Ono et al. (2014) in this volume.

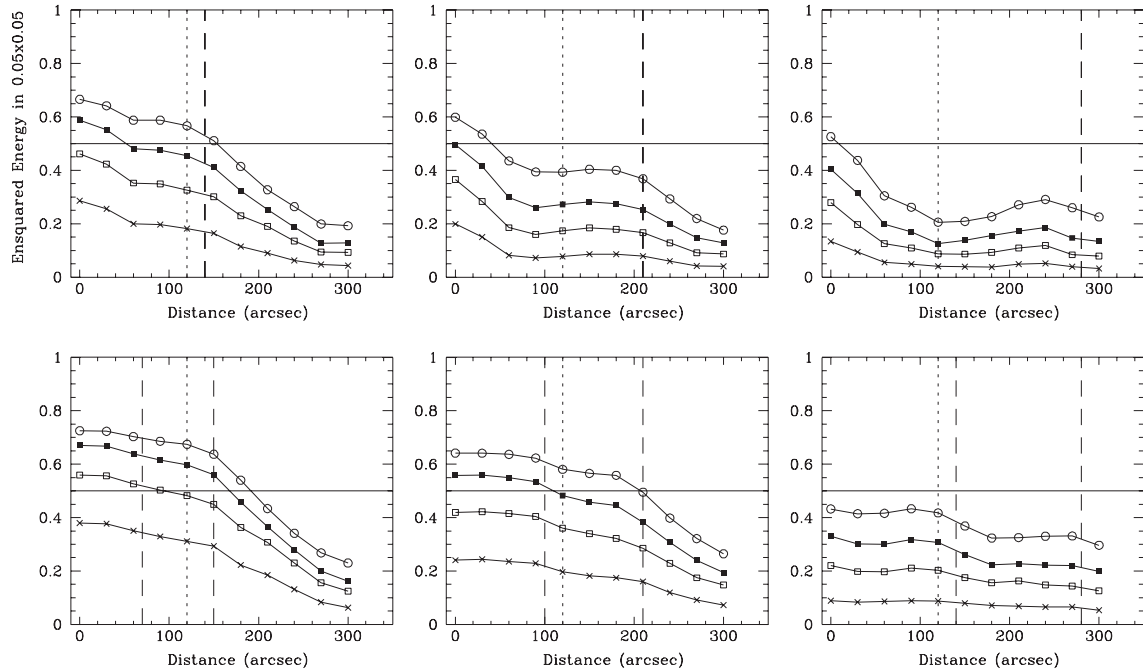


Figure 6. EE within  $0.05'' \times 0.05''$  aperture as a function of distance from the FoR center. Crosses, open-squares, filled-squares, and open circles represent EE in the  $0.9\mu\text{m}$ ,  $J$ -,  $H$ -, and  $K$ -bands, respectively. The vertical dashed and dotted lines represent radius of LGSs and NGSs asterism. The lower left panel corresponds to the nominal TMT-IRMOS configuration.

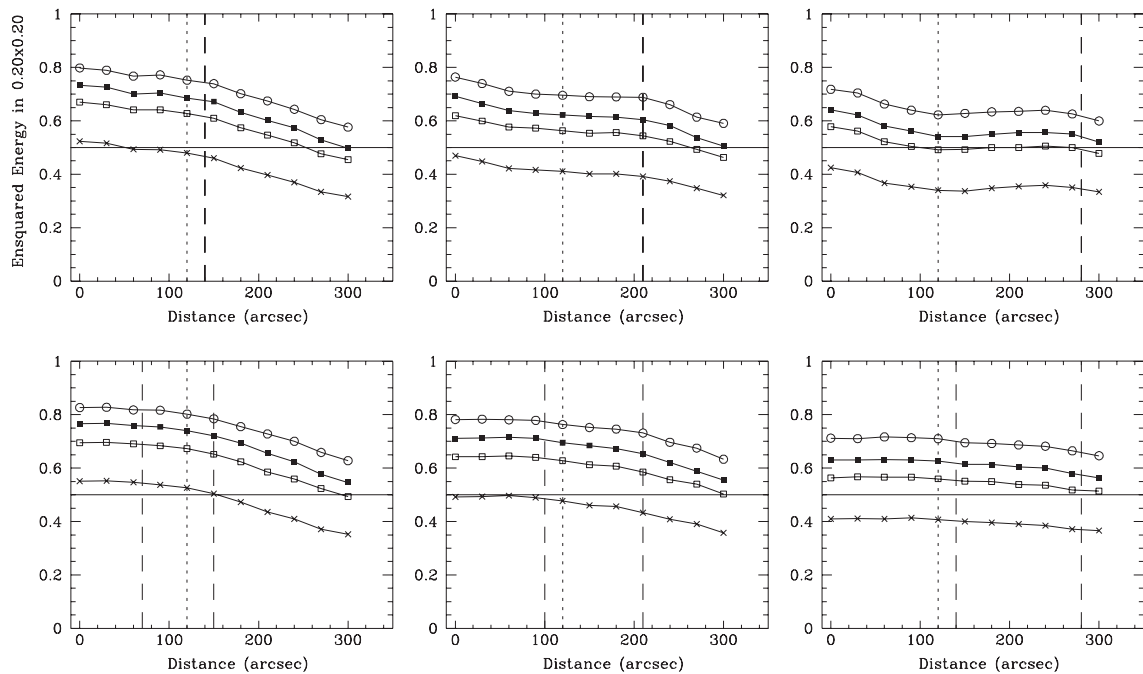


Figure 7. Same as Figure 6 for  $0.20'' \times 0.20''$  aperture.

### 3. OVERALL SYSTEM CONSIDERATION

#### 3.1 MOAO system design and requirements for DM

Large optical path difference within 30m aperture due to the atmospheric turbulence demands large stroke for DMs in TMT AO system. Requirements for the DM stroke are critical system constraints on an MOAO system design for ELTs. In order to achieve the close to diffraction limited PSF, at least  $60 \times 60$  DM covering the 30m aperture is necessary for each science path, but the mechanical stroke for such large element number DM is still limited.

We evaluate requirements for the mechanical stroke of the DM in an MOAO system through numerical simulations with AO simulation code developed by one of the authors (Y.O.). In the results below, we assume moderate condition with seeing of  $r_0 = 0.156\text{m}$  and zenith angle of 0 deg, and bad condition with seeing of  $r_0 = 0.121\text{m}$  and zenith angle of 60 deg (equivalent to  $r_0 = 0.08\text{m}$  at zenith) with 7 layer atmosphere models of Mauna Kea.<sup>23</sup> We derive two values for each condition and setup, one is the Peak-to-Valley (PV) stroke value of low spatial frequency mode for each DM sampling after removal of the TT component, and the other is the maximum inter-actuator (IA) stroke which is the difference between neighbouring actuators. Resulting values below represent mechanical stroke and are half of the corresponding values of the wavefront optical path difference. These values are derived as an upper  $2\sigma$  envelope of 100 simulations for each condition and setup. If all of the wavefront distortion component is corrected by one  $60 \times 60$  DM, we require  $5.5\mu\text{m}$  PV stroke and  $2.5\mu\text{m}$  IA stroke for the moderate condition and  $10.0\mu\text{m}$  PV stroke and  $4.0\mu\text{m}$  IA stroke for the bad condition, they are consistent with previous estimates.<sup>22</sup> These values are significantly larger than the currently available 30mm-size >3000-elements MEMS DM. For example, 4092-elements MEMS DM from Boston Micromachines have  $3.5\mu\text{m}$  PV stroke and  $1.5\mu\text{m}$  IA stroke.<sup>24</sup>

One way to fulfill the stroke requirements is using the Woofer-Tweeter DMs in each science path. Woofer-DM corrects for low-spatial frequency modes with large amplitudes and following Tweeter-DM corrects for high-spatial frequency modes with small amplitude. If we assume  $30 \times 30$  DM as a Woofer-DM, the required strokes for the Woofer-DM are  $5.5\mu\text{m}$  PV and  $2.5\mu\text{m}$  IA strokes for the moderate condition and  $10.0\mu\text{m}$  PV and  $4.5\mu\text{m}$  IA strokes for the bad condition. Most of the required strokes for the Woofer-DM, except for the IA stroke under bad condition, can be fulfilled by the currently available small-size DMs, for example, 277-element electromagnetic DM from ALPAO ([www.alpao.fr](http://www.alpao.fr)) have  $25\mu\text{m}$  Tip-Tilt and  $3.0\mu\text{m}$  inter-actuator strokes. The number of elements needs to be increased to meet the  $30 \times 30$  requirement. In this case, the strokes of the Tweeter DM for correcting the remaining high spatial frequency modes are  $1.0\mu\text{m}$  ( $2.0\mu\text{m}$ ) PV and  $1.0\mu\text{m}$  ( $1.5\mu\text{m}$ ) IA for the moderate (bad) condition. Currently available MEMS DM realize all of the stroke requirements.

Another solution for the stroke requirements is proposed in IRMOS-Tipi feasibility study. In the design, modified Offner relay is inserted before the pick-off optics for each science path. The secondary mirror of the modified Offner relay is a DM that corrects the common wavefront distortion in all of the science path. The residual wavefront distortion for each science path is corrected by an individual DM in each science path. We calculate the stroke requirements for the common DM and DM in each science path. We assume the common DM corrects average wavefront distortion measured by the multiple LGSs and works like a GLAO system. In this calculation the strokes  $5'$  away from the center is considered, but the difference in the stroke requirements in small FoR is small, less than  $1\mu\text{m}$ . The number of elements in the common DM affects the stroke requirements of the individual DM. If the number of elements in the common DM becomes larger up to  $30 \times 30$ , the required stroke for the individual DM gets smaller. The trend saturate at  $30 \times 30$  and increasing the number of elements above  $30 \times 30$  do not reduce the required stroke for the individual DM. Therefore, we choose  $30 \times 30$  elements for the common DM. In this case, the requirements for the common DM is  $5.0\mu\text{m}$  ( $8.0\mu\text{m}$ ) PV and  $2.5\mu\text{m}$  ( $3.5\mu\text{m}$ ) IA strokes for moderate (bad) condition. For the individual DM, the requirements are  $3.0\mu\text{m}$  ( $5.5\mu\text{m}$ ) PV and  $1.0$  ( $2.0\mu\text{m}$ ) IA strokes for moderate (bad) condition. Because the common DM can be as large as 300-400mm diameter depending on the optical design, the required large stroke can be fulfilled with the piezo-stack DM. The requirements for the PV stroke of the individual DM is larger than the Woofer-Tweeter case, because low-order distortion modes of high altitude atmospheric layers are not corrected by the common DM. The required PV stroke is larger than the stroke of the currently available MEMS DM.

The above stroke requirements for the DMs are summarised in Table 2.

Table 2. Requirements for DM PV and inter-actuator strokes in three different systems in  $\mu\text{m}$ . Values are upper  $2\sigma$  values of 100 simulations with the moderate condition. Values in parenthesis are for the bad conditions. Tip-tilt component is not included.

System	30×30 DM		60×60 DM	
	PV	IA	PV	IA
One 60 × 60 DM for each path	—	—	5.5 (10.0)	2.5 (4.0)
30 × 30 Woofer- 60 × 60 Tweeter DMs for each path	5.5 (10.0)	2.5 (4.5)	1.0 (2.0)	1.0 (1.5)
Common 30 × 30 DM and one 60 × 60 DM for each path	5.0 (8.0)	2.5 (3.5)	3.0 (5.5)	1.0 (2.0)

### 3.2 Optical design for a common DM system

The common DM design can have a few advantages over the Woofer-Tweeter system in each science path,<sup>3</sup> especially, part of the AO correction can be applied in closed-loop and images of the TT-guide stars can be partly corrected. Such correction for TT-guide star can improve the limiting magnitude of TT WFS and increase the sky coverage of the system. Considering the advantages, though the required PV strokes for the 60 × 60 DMs are larger than that of Woofer-Tweeter system and that of the currently available MEMS DMs, we further investigate the feasibility of the common DM system of 10' diameter FoR in the optical design point of view.

One extreme case of the common DM system is using the adaptive secondary mirror as the common DM. Adaptive secondary mirror is considered as a possible future upgrade in the TMT project.<sup>3</sup> Considering the difficulty associated with fabricating the adaptive secondary mirror with 3.0m diameter, we do not further evaluate the possibility in this study.

At first, we consider modified Offner system following the IRMOS-Tipi feasibility study. In the optical design, the common DM is conjugated to the primary mirror. We put emphasis on the size of the blur of the pupil image on the common DM; it should be as small as half of the subaperture of 30×30 common DM, i.e. 1.7%, within 5' diameter FoR, and as small as the subaperture, i.e. 3.3%, within 10' diameter FoR. Strictly speaking, pupil shift with 17% of subaperture size can introduce wavefront residual as large as fitting error of 30×30 DM, that means, the blur of the pupil image is better to be as small as 0.6%. The effect of the blur of the pupil to the performance inside wide FoR should be examined following the optical designs in the future. One optical design by Optcraft (T.Y.) is shown in the left panel of Figure 8. In the optical design, the primary mirror of the modified Offner relay is spherical and has diameter of 4720mm. The secondary mirror corresponds to the common DM and has diameter of 400mm. The secondary mirror is also spherical and has curvature. In this design, small glass plates in front of the focal plane are inserted to correct astigmatism for each science direction individually. Such correction can be made by the individual DM in each science path, but the PV value of the wavefront distortion is  $5.8\mu\text{m}$  at the edge of the FoR and consume the stroke of the individual DM. The blur of the pupil on the common DM meet the specification, less than 1.7% in most of the FoR except for the upper edge of 10' FoR. The overall size of the design is 8436mm and close to the limit of the TMT Nasmyth platform accepting 10m length system.

In order to reduce the size of the entire system, as well as the size of the largest optical component, we also consider an optical design with free curve mirrors. The optical design by Photocoding (Y.I.) is shown in the right panel of Figure 8. In this design, all of the mirrors are free form curve except for the flat DM. The resulting size of the envelope is about half of that of the modified Offner design. The largest mirror has 1.7m diameter and the DM has 280mm diameter. The distortion at the focal plane is within  $\pm 1.5\mu\text{m}$ . The blur of the pupil on the common DM is 11% at most for the edge of the FoR. The blur is larger than the specification at the edge.

In summary, there is an optical design for the common DM AO foreoptics that meets the requirements in the 10' FoR. Further opt-mechanical consideration of the system will be made as a next step.

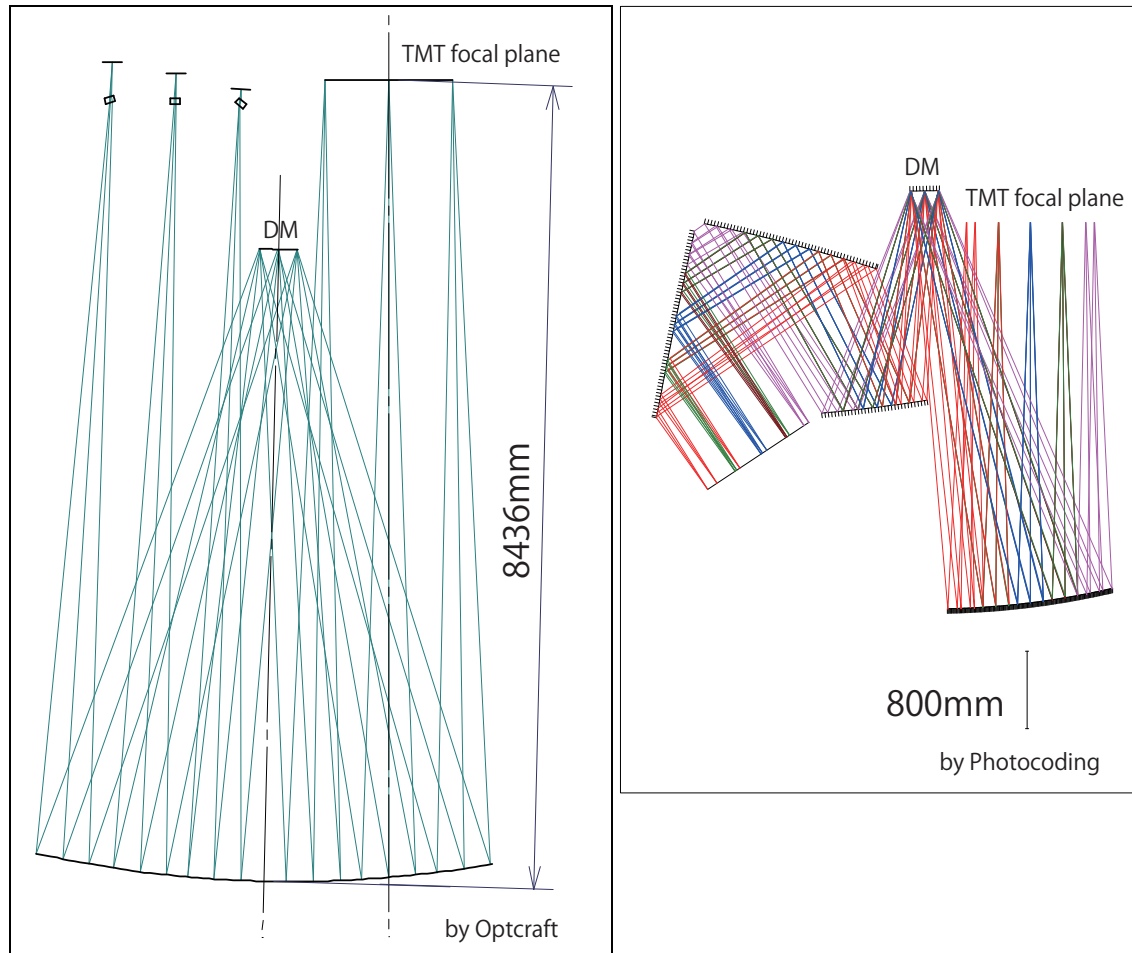


Figure 8. The optical design for the common DM AO optics. Left) modified Offner design by Optcraft. Right) Free curve mirror array design by Photocoding.

## 4. DEVELOPMENTS FOR INDIVIDUAL COMPONENT

### 4.1 Requirements for high-dynamic range wavefront sensor

Because wavefront measurements in an MOAO system are done in open-loop manner, required dynamic range for LGS WFS in the MOAO system is larger than a WFS in a closed-loop system. Assuming Shack-Hartmann (SH) WFS,  $5''$  FoV per subaperture is necessary to cover 5-sigma scatter of the wondering of spots under bad seeing condition with  $r_0 = 0.08\text{m}$  and measurement wavelength of  $589\text{nm}$ . If we assume each spot of  $60 \times 60$  SH WFS has  $900 e^-$ , which is the specified brightness of LGS for NFIRAOS,<sup>18</sup> simple simulation with threshold-centroiding suggests that pixel sampling of  $0.25''$  is necessary to determine the position of each spot with  $1\sigma$  accuracy of  $0.01''$ . If we simulate the wavefront reconstruction through SH LGS WFS with  $30\text{m}$  aperture considering the spot elongation due to the Na-layer height profile,  $0.4'' - 0.5''$  sampling is the optimised sampling for  $60 \times 60$  LGS WFS. With the setup, wavefront reconstruction accuracy is  $150\text{nm}$  rms WFE including fitting error. Therefore, we require at least  $10 \times 10$  pixels for each subaperture and  $600 \times 600$  pixels in total.

### 4.2 Large stroke MEMS deformable mirror

As summarised in Section 3.1, the strokes of the currently available MEMS DMs cannot meet the required specification for  $60 \times 60$  DM inside the common DM system design. In order to realize the large stroke MEMS DM, we are conducting a development of a large stroke ( $20\mu\text{m}$ ) MEMS deformable mirror.<sup>22,25-27</sup> We propose a

new MEMS structure design with a bimorph-spring structure made by a  $\text{HfO}_2$  crystallisation process and Au-Si eutectic bonding process. We fabricated  $2 \times 2$  and  $4 \times 4$  elements prototypes with  $200\mu\text{m}$  length bimorph springs and  $500\mu\text{m}$  spacing. By the bimorph-spring structure, the gap between the facesheet and the electrode as wide as  $20\mu\text{m}$  can be realized. The  $2 \times 2$  prototype shows  $7.6\mu\text{m}$  PV stroke with 110V and  $4 \times 4$  prototype shows  $3.5\mu\text{m}$  PV stroke with 115V voltage. The response time of the DM is less than 0.5ms. The details of the structure and results are shown in Wu et al. (2013).<sup>27</sup>

### 4.3 Tomography calculation with GPGPU

Fast tomographic reconstruction within 1ms is another key component of an MOAO system. In order to realize the fast tomographic reconstruction, we apply parallel calculation with General Purpose Graphic Processor Unit (GPGPU). The required time for the tomographic reconstruction with GPGPU through AO simulation is evaluated. In the simulation, atmospheric turbulence structure in 7 layers is estimated by 8  $60 \times 60$  LGS WFSs measurements. The estimation is derived based on the minimum variance solution of the tomographic reconstruction solved by conjugate gradient method (CG method).<sup>23</sup>

We use NVIDIA GTX Titan to solve the tomographic reconstruction in the simulation. One iteration of the CG method takes 0.7ms with the current setup. The solution converges with 300 iterations with the CG method, and it takes about 200ms in total to determine the solution. The required time is much longer than the specification currently. However the required number of iterations can be reduced to several times by using the solution from the previous time step as the initial guess. Therefore improvement with the initial guess and further speed up of the GPGPU processing may meet the specification.

The required time for data transfer from and to GPGPU can be another bottleneck for the fast tomography reconstruction. Through the current setup with PCIe2.0 bus, transferring slope data to GPGPU and transferring reconstructed solution from GPGPU take 0.2ms and 0.4ms, respectively. We confirmed that the required time for data transfer can be reduced with using PCIe3.0 bus by factor of 1.5.

## 5. SUMMARY

We introduce current status of the feasibility study on a wide FoR MOAO system for TMT (TMT-AGE). In this study, we put emphasise on the FoR as wide as  $10'$  diameter. The wide FoR is crucial to effectively observe very high-redshift galaxies at  $z > 5$ , which have low surface number density.

Simulations of an MOAO system show close-to-diffraction-limited correction can be achieved within  $5'$  diameter FoR with 8 LGSs located within  $140''$ . Furthermore, moderate AO correction can be achieved within  $10'$  diameter FoR with the same LGS asterism. The EE within  $0.2'' \times 0.2''$  can be 2.5 times larger than the seeing-limited case within the FoR.

We discuss overall system design of the wide FoR MOAO system considering the constraint of the stroke of small-size deformable mirror DM. We compare the stroke requirements for DM in the Woofer-Tweeter system and in the common DM system. In the common DM system, required PV stroke is larger than Woofer-Tweeter system. We show two optical designs for the common DM system, one based on modified Offner relay and the other one based on three mirror array of free curve surfaces.

We also introduce current status of developments of key components of an MOAO system; high-dynamic range WFS, large-stroke small-size MEMS DM, and fast tomographic reconstruction RTC with GPGPU.

## ACKNOWLEDGMENTS

This work is supported by Japanese TMT office strategic research and development funding of FY2012, FY2013, and FY2014. M.A. is supported by JSPS KAKENHI Grant-in-Aid for Young Scientists (B) 23740140 and Grant-in-Aid for Scientific Research (B) 26287027.

## REFERENCES

- [1] Hammer, F., Puech, M., Assemat, F., and et al., “FALCON: a concept to extend adaptive optics corrections to cosmological fields,” in [*Second Backaskog Workshop on Extremely Large Telescopes*], *Proc. SPIE* **5382** (2004).
- [2] Rousset, G., Fusco, T., Assemat, F., Gendron, E., Morris, T., Robert, C., Myers, R., Cohen, M., Dipper, N., Evans, C., Gratadour, D., Jagourel, P., Laporte, P., Le Mignant, D., Puech, M., Schnetler, H., Taylor, W., Vidal, F., Cuby, J.-G., Lehnert, M., Morris, S., and Parr-Burman, P., “EAGLE MOAO system conceptual design and related technologies,” in [*Adaptive Optics Systems II*], *Proc. SPIE* **7736** (2010).
- [3] Crampton, D. and Simard, L., “Instrument concepts and scientific opportunities for TMT,” in [*Ground-based and Airborne Instrumentation for Astronomy*], *Proc. SPIE* **6269** (2006).
- [4] Eikenberry, S., Andersen, D., Guzman, R., Bally, J., Cuevas, S., Fletcher, M., Gardhouse, R., Gavel, D., Gonzalez, A., Gruel, N., Hamann, F., Hamner, S., Julian, R., Julian, J., Koo, D., Lada, E., Leckie, B., Lopez, J. A., Pello, R., Perez, J., Rambold, W., Roman, C., Sarajedini, A., Tan, J., Venn, K., Veran, J.-P., and Ziegert, J., “IRMOS: The near-infrared multi-object spectrograph for the TMT,” in [*Ground-based and Airborne Instrumentation for Astronomy*], *Proc. SPIE* **6269** (2006).
- [5] Andersen, D. R., Eikenberry, S. S., Fletcher, M., Gardhouse, W., Leckie, B., Véran, J.-P., Gavel, D., Clare, R., Guzman, R., Jolissaint, L., Julian, R., and Rambold, W., “The MOAO system of the IRMOS near-infrared multi-object spectrograph for TMT,” in [*Ground-based and Airborne Instrumentation for Astronomy*], *Proc. SPIE* **6269** (2006).
- [6] Gavel, D., Bauman, B., Dekany, R., Britton, M., and Andersen, D., “Adaptive optics designs for an infrared multi-object spectrograph on TMT,” in [*Advances in Adaptive Optics II*], *Proc. SPIE* **6272** (2006).
- [7] Taylor, K., Britton, M. C., Moore, A. M., and et al., “Tipi: A deployable integral-field spectrograph concept for TMT,” in [*Ground-based and Airborne Instrumentation for Astronomy*], *Proc. SPIE* **6269** (2006).
- [8] Shapley, A. E., Steidel, C. C., Pettini, M., and Adelberger, K. L., “Rest-Frame Ultraviolet Spectra of  $z \sim 3$  Lyman Break Galaxies,” *Astrophysical Journal* **588**, 65–89 (2003).
- [9] Martin, C. L., Shapley, A. E., Coil, A. L., Kornei, K. A., Bundy, K., Weiner, B. J., Noeske, K. G., and Schiminovich, D., “Demographics and Physical Properties of Gas Outflows/Inflows at  $0.4 < z < 1.4$ ,” *Astrophysical Journal* **760**, 127 (2012).
- [10] Akiyama, M., Minowa, Y., Kobayashi, N., Ohta, K., Ando, M., and Iwata, I., “Adaptive Optics Rest-Frame V-Band Imaging of Lyman Break Galaxies at  $z \sim 3$ : High Surface Density Disklike Galaxies?,” *Astrophysical Journal Supplement Series* **175**, 1–28 (2008).
- [11] Förster Schreiber, N. M., Genzel, R., Bouché, N., Cresci, G., Davies, R., Buschkamp, P., Shapiro, K., Tacconi, L. J., Hicks, E. K. S., Genel, S., Shapley, A. E., Erb, D. K., Steidel, C. C., Lutz, D., Eisenhauer, F., Gillessen, S., Sternberg, A., Renzini, A., Cimatti, A., Daddi, E., Kurk, J., Lilly, S., Kong, X., Lehnert, M. D., Nesvadba, N., Verma, A., McCracken, H., Arimoto, N., Mignoli, M., and Onodera, M., “The SINS Survey: SINFONI Integral Field Spectroscopy of  $z \sim 2$  Star-forming Galaxies,” *Astrophysical Journal* **706**, 1364–1428 (2009).
- [12] Bouwens, R. J., Illingworth, G. D., Blakeslee, J. P., Broadhurst, T. J., and Franx, M., “Galaxy Size Evolution at High Redshift and Surface Brightness Selection Effects: Constraints from the Hubble Ultra Deep Field,” *Astrophysical Journal Letters* **611**, L1–L4 (2004).
- [13] Stark, D. P., Swinbank, A. M., Ellis, R. S., Dye, S., Smail, I. R., and Richard, J., “The formation and assembly of a typical star-forming galaxy at redshift  $z \sim 3$ ,” *Nature* **455**, 775–777 (2008).
- [14] Ono, Y., Ouchi, M., Curtis-Lake, E., Schenker, M. A., Ellis, R. S., McLure, R. J., Dunlop, J. S., Robertson, B. E., Koekemoer, A. M., Bowler, R. A. A., Rogers, A. B., Schneider, E., Charlot, S., Stark, D. P., Shimasaku, K., Furlanetto, S. R., and Cirasuolo, M., “Evolution of the Sizes of Galaxies over  $7 < z < 12$  Revealed by the 2012 Hubble Ultra Deep Field Campaign,” *Astrophysical Journal* **777**, 155 (2013).
- [15] Konno, A., Ouchi, M., Ono, Y., Shimasaku, K., Shibuya, T., Furusawa, H., Nakajima, K., Naito, Y., Momose, R., Yuma, S., and Iye, M., “Accelerated Evolution of Ly $\alpha$  Luminosity Function at  $z \sim 7$  Revealed by the Subaru Ultra-Deep Survey for Ly $\alpha$  Emitters at  $z = 7.3$ ,” *submitted to Astrophysical Journal*, arXiv:1404.6066 (2014).

- [16] Bouwens, R. J., Illingworth, G. D., Oesch, P. A., Trenti, M., Labbe', I., Bradley, L., Carollo, M., van Dokkum, P. G., Gonzalez, V., Holwerda, B., Franx, M., Spitler, L., Smit, R., and Magee, D., "UV Luminosity Functions at redshifts  $z \sim 4$  to  $z \sim 10$ : 11000 Galaxies from HST Legacy Fields," *submitted to Astrophysical Journal*, arXiv:1403.4295 (2014).
- [17] Herriot, G., Andersen, D., Atwood, J., Byrnes, P., Boucher, M.-A., Boyer, C., Caputa, K., Correia, C., Dunn, J., Ellerbroek, B., Fitzsimmons, J., Gilles, L., Hickson, P., Hill, A., Kerley, D., Pazder, J., Reshetov, V., Roberts, S., Smith, M., Véran, J.-P., Wang, L., and Wevers, I., "TMT NFIRAOS: adaptive optics system for the Thirty Meter Telescope," in [*Adaptive Optics Systems III.*], *Proc. SPIE* **8447** (2012).
- [18] Boyer, C., Ellerbroek, B., Gedig, M., Hileman, E., Joyce, R., and Liang, M., "Update on the TMT laser guide star facility design," in [*Adaptive Optics Systems*], *Proc. SPIE* **7015** (2008).
- [19] Girardi, L., Groenewegen, M. A. T., Hatziminaoglou, E., and da Costa, L., "Star counts in the Galaxy. Simulating from very deep to very shallow photometric surveys with the TRILEGAL code," *Astronomy and Astrophysics* **436**, 895–915 (2005).
- [20] Wang, L. and Ellerbroek, B. in [*Adaptive Optics Systems III.*], *Proc. SPIE* **8447** (2012).
- [21] Chun, M., Wilson, R., Avila, R., Butterley, T., Aviles, J.-L., Wier, D., and Benigni, S., "Mauna Kea ground-layer characterization campaign," *Monthly Notices of the Royal Astronomical Society* **394**, 1121–1130 (2009).
- [22] Akiyama, M., Oya, S., Hane, K., Wu, T., and Tokoku, C., "MOAO activities in Tohoku university," in [*Adaptive Optics Systems II.*], *Proc. SPIE* **7736** (2010).
- [23] Ono, Y. H., Akiyama, M., and Oya, S., "TMT-AGE: numerical simulation of a new tomographic reconstruction method for wide FoR MOAO," in [*Adaptive Optics System IV*], *Proc. SPIE in this volume* (2014).
- [24] Cornelissen, S. A., Hartzell, A. L., Stewart, J. B., Bifano, T. G., and Bierden, P. A., "MEMS deformable mirrors for astronomical adaptive optics," in [*Adaptive Optics Systems II.*], *Proc. SPIE* **7736** (2010).
- [25] Wu, T., Akiyama, M., and Hane, K., "Continuous membrane deformable mirror for adaptive optics using bimorph spring," in [*Solid State Sensors, Actuators, and Microsystems*], *Proc. IEEE Conf.* (2011).
- [26] Akiyama, M., Ono, Y. H., Oya, S., Hane, K., and Wu, T., "MOAO test bench in Tohoku university," in [*Adaptive Optics Systems III.*], *Proc. SPIE* **8447** (2012).
- [27] Wu, T., Sasaki, T., Akiyama, M., and Hane, K., "Large-scale membrane transfer process: its application to single-crystal-silicon continuous membrane deformable mirror," *J. Micromech. Microeng.* **23**, 125003.